Prospects of the WSR-88D Radar for Cloud Studies

VALERY M. MELNIKOV

Cooperative Institute for Mesoscale Meteorological Studies, University of Oklahoma, Norman, Oklahoma

DUSAN S. ZRNIĆ AND RICHARD J. DOVIAK

NOAA/OAR/National Severe Storms Laboratory, Norman, Oklahoma

PHILLIP B. CHILSON

School of Meteorology and Atmospheric Radar Research Center, University of Oklahoma, Norman, Oklahoma

DAVID B. MECHEM

Atmospheric Science Program, Department of Geography, University of Kansas, Lawrence, Kansas

YEFIM L. KOGAN

Cooperative Institute for Mesoscale Meteorological Studies, University of Oklahoma, Norman, Oklahoma

(Manuscript received 1 June 2009, in final form 21 March 2010)

ABSTRACT

Sounding of nonprecipitating clouds with the 10-cm wavelength Weather Surveillance Radar-1988 Doppler (WSR-88D) is discussed. Readily available enhancements to signal processing and volume coverage patterns of the WSR-88D allow observations of a variety of clouds with reflectivities as low as −25 dBZ (at a range of 10 km). The high sensitivity of the WSR-88D, its wide velocity and unambiguous range intervals, and the absence of attenuation allow accurate measurements of the reflectivity factor, Doppler velocity, and spectrum width fields in clouds to ranges of about 50 km. Fields of polarimetric variables in clouds, observed with a research polarimetric WSR-88D, demonstrate an abundance of information and help to resolve Bragg and particulate scatter. The scanning, Doppler, and polarimetric capabilities of the WSR-88D allow real-time, three-dimensional mapping of cloud processes, such as transformations of hydrometeors between liquid and ice phases. The presence of ice particles is revealed by high differential reflectivities and the lack of correlation between reflectivity and differential reflectivity in clouds in contrast to that found for rain. Pockets of high differential reflectivities are frequently observed in clouds; maximal values of differential reflectivity exceed 8 dB, far above the level observed in rain. The establishment of the WSR-88D network consisting of 157 polarimetric radars can be used to collect cloud data at any radar site, making the network a potentially powerful tool for climatic studies.

1. Introduction

Clouds cycle water and energy through the atmosphere and play a vital role in determining the global radiation balance. A large amount of cloud data has been obtained with millimeter-wavelength radars. The use of short wavelengths makes it possible to achieve a very high level of spatial resolution with relatively small antennas and to provide good detectability of nonprecipitating clouds. Kollias et al. (2007) recently published a review of ground-based cloud radars and their applications (see also Hamazu et al. 2003; Manheimer et al. 2003; Widener and Mead 2004). Continuously running millimeter-wavelength cloud radars (MMCRs), operated by the Atmospheric Radiation Measurement Program (ARM), have vertically pointed beams so they obtain cloud parameters above the radars. There are two types of MMCRs, which we will be referring to as MMCR-8 and MMCR-3: the first operates at an 8-mm

Corresponding author address: Dr. Valery Melnikov, CIMMS, University of Oklahoma, 120 David Boren Blvd., Rm. 4919, Norman, OK 73072.
E-mail: valery.melnikov@noaa.gov

DOI: 10.1175/2010JAMC2303.1

wavelength and the second at a 3-mm wavelength. Retrievals of cloud parameters using MMCRs can be found in Kropfli and Kelly (1996), Clothiaux et al. (1995), Kollias et al. (2001), Matrosov et al. (1992, 2002), and Reinking et al. (2002), among others.

In April 2006, the Cloud Profiling Radar (CPR) was put into orbit as part of the *CloudSat* mission. The CPR is a 3-mm-wavelength radar developed in order to collect global data from clouds (Stephens et al. 2002). The CPR has demonstrated unique capabilities for cloud mapping, but its data have severe limitations in spatial resolution, the number of measurement parameters, and update time. These limitations will be difficult to overcome in the foreseeable future.

The National Weather Service (NWS) operates a network of 10-cm-wavelength WSR-88Ds; the network has 157 units. This network has been designed to monitor severe weather and precipitation. As such, existing radar volume coverage patterns (VCPs) have been optimized for those purposes. The maximum elevation angle of the VCPs is about 20° and the signal-to-noise ratio (SNR) threshold for reflectivity displays is typically set to 2 dB. All of these factors constructively combine to inhibit the detection of echoes from nonprecipitating clouds. We show that the high-power transmitters, low-noise receivers, and readily available enhancements to signal processing give the WSR-88D an inherent capability to detect a variety of nonprecipitating clouds.

Miller et al. (1998) arrived at mixed results when comparing cloud detections using a WSR-88D from the NWS network and those detections obtained with a vertically pointed 3-mm-wavelength cloud radar. Both radars detected clouds up to 80% of the time during a 2-month campaign; sometimes, the WSR-88D registered echoes that had not been registered with the 3-mm-wavelength radar and vice versa. Miller et al. show that significant obstacles impair the collection of cloud data with a WSR-88D using available algorithms. But we were able to operate the National Severe Storms Laboratory's (NSSL's) Research and Development WSR-88D in a mode that overcame many of these obstacles to demonstrate the inherent capabilities of this radar for cloud measurements. Furthermore, we discuss how upcoming polarimetric upgrades to the WSR-88D can help resolve some of the ambiguities that plagued the measurements made by Miller et al. (1998).

In section 2, we compare the theoretical performance of the NSSL WSR-88D (i.e., KOUN, located in Norman, Oklahoma) with that obtained with the MMCRs being used for continuous data collection [i.e., ARM's MMCR-8 and MMCR-3, and the CPR operated by the National Aeronautics and Space Administration (NASA)]. We also compare cloud observations made with a network WSR-88D to those made at KOUN (i.e., a polarimetric WSR-88D). Polarimetric capabilities will be added to the network of WSR-88Ds in the near future. In section 3, we demonstrate the importance of a large unambiguous velocity interval and low attenuation rates for quantitative cloud measurements. In section 4, we present the first results of polarimetric radar observations in nonprecipitating clouds conducted at KOUN. We also demonstrate the importance of low attenuation rates for quantitative polarimetric measurements. In section 5, we discuss how dual-wavelength polarimetric data can help to resolve the relative contributions from incoherent and coherent scatter.

2. KOUN signal processing for cloud observations

WSR-88Ds are operated in two surveillance modes: "clear air" and "precipitation." The clear-air mode is used in fair weather to monitor the possible development of precipitation. In this mode, a microwave pulse of longer length (4.5 μs) is transmitted to improve the detection of weak echoes. Upon detecting echoes above a selected reflectivity factor threshold, the radar automatically switches over to the precipitation mode that uses the shorter-length pulse (1.57 μs). To stipulate cloud detection capabilities, two parameters are most significant: 1) the reflectivity factor Z_{10} that produces an echo SNR = 0 dB at a range of 10 km and 2) range resolution, ΔR. The Z_{10} in the precipitation mode is -21.5 dBZ (Doviak and Zrnić 2006, Table 3.1); in the clear-air mode sensitivity is 9.5 dB better but ΔR is about 750 m. So there is the likelihood that the number of scatterers will not increase proportionally with ΔR, a required condition necessary to achieve the 9.5-dB sensitivity increase. This condition is less likely to be met for observations of thin cloud layers at high-elevation angles. For this reason, we have restricted our observations to the short pulse mode.

To enhance quantitative measurements of clouds, the following data collection and signal processing procedures were used:

1) longer dwell times (i.e., 128 samples spaced about 1 ms apart, about 3 times that typically used by the NWS) to improve the accuracy of the measurements,
2) smaller elevation increments (i.e., 0.25° instead of 1°) to improve the accuracy and number of measurements,
3) twice the range sampling rate, also to improve accuracy,
4) a noise speckle remover to reduce the occurrence of false echoes,
5) correlation estimators for polarimetric variables to lessen noise effects,

TABLE 1. Parameters of radars selected for cloud measurement; GSM and CM stand for the general and stratus and cirrus modes of operations, respectively.

	ARM's MMCR-8	ARM's MMCR-3	NASA's CPR	NOAA's WSR-88D (short-pulse mode)
Wavelength (mm)	8.7	3	3	109
Pulse power (kW)	0.1	1.7	—	450
Pulse width (μs)	0.3/0.6	0.3	3.3	1.57
Antenna size (m)	3	0.6	1.95	8.54
Beamwidth (one-way half-power width,°)	0.2	0.24	0.12	0.96
Radial resolution (m)	45/90	45	500	250
Two-way transversal resolution (m)	10 at 10 km	17 at 10 km	1400 (cross track), 2500 (along track)	49 at 10 km
Z_{10} (dBZ)	−30 (GSM) −48 (CM)	−26	−26	−21.5 (single polarization) −18.5 (dual polarization) −25.5 (with enhanced processing in dual-polarization mode)
Scanning capability	No	No	No	Yes
Doppler capability	Yes	Yes	No	Yes
Unambiguous velocity (m s^{-1})/range of measurements (km)	3.2/16 (GSM), 20.3/16 (CM)	7.9/15	—	27/150–35/117
Dual polarization	Yes, for the Southern Great Plains site	Yes	No	Yes, for KOUN; yes, for upgraded WSR-88Ds
Attenuation	Strong	Severe	Severe	Negligible
No. of systems	5	3	1	157

6) data collection at elevations higher than 20° to observe clouds at close range, and
7) ground clutter filters at all elevations to remove many artifacts.

Procedures 1–5 improve the accuracy of the presented data and provide images that are less cluttered by noise and artifacts. We collected cloud data at elevations angles up to 60°, the elevation limit for the WSR-88D. These data collection and processing procedures allow clear data presentations at SNRs as low as −7 dB. Herein, we present radar images as vertical cross sections or range–height indicators (RHIs). At the pulse repetition frequency (PRF) of 1280 Hz, 24 s is needed to complete one RHI with procedures 1–7 above. For the KOUN radar, Z_{10}, presented in the nonpolarimetric mode, is −21.5 dBZ (Table 1). Radar products from the network WSR-88D are generated if the SNR is larger than 2 dB. Thus, we present reflectivity data 9 dB lower than that typically used by the NWS. The standard deviation {i.e., SD[$\hat{Z}$(dBZ)]} of the reflectivity factor estimate for a radar resolution volume (i.e., 1° × 0.25 km) producing an SNR of −7 dB is $\mathrm{SD}(\hat{Z}) = 4.34/(M^{1/2}\mathrm{SNR})[1 + 2\mathrm{SNR} + \mathrm{SNR}^2/(2\sigma_{vn}\pi^{1/2})]^{1/2}$ dBZ, where $\sigma_{vn} = \sigma_v/(2v_a)$ and v_a is the unambiguous velocity (Doviak and Zrnić 2006; section 6.3.1.2). For an SNR = 0.2 (−7 dB), σ_v = 1 m s^{-1}, and M = 768, (i.e., 128 time samples, multiplied by the 4 angular and 1.5 range samples), we obtain SD($\hat{Z}$) = 1.0 dBZ.

Several of the significant parameters of some cloud radars and the WSR-88D are listed in Table 1. The 8-mm-wavelength radars are capable of resolving many of the structures found within clouds of varying thickness (Moran et al. 1998). Although the MMCR-3 radars are well suited for cloud observations, attenuation becomes an issue. As can be seen in Table 1, the minimum measurable reflectivity that will be available from the upgraded polarimetric WSR-88D is about the same as that for the 3-mm MMCRs, and about 5 dB worse than that for the MMCR-8 in the general mode. Thus, the detectability of clouds by the WSR-88D is comparable to that of the cloud radars. But the ground-base cloud radars are superior by a factor of 3–5 to the WSR-88D in spatial resolution (Table 1).

Figures 1 and 2 demonstrate the capability of the KOUN radar to detect optically thin clouds. Sky pictures to the west and east of KOUN are presented in Figs. 1a and 1b, the composite reflectivity (i.e., maximal reflectivities for all elevations) from the NWS WSR-88D 11 km northeast of KOUN near Oklahoma City (KTLX) is shown in Fig. 1c, and a visible satellite image over Oklahoma is presented in Fig. 1d. Cirrus clouds in central Oklahoma are barely seen in Fig. 1d, and it is impossible to discern the presence of cirrus clouds in Fig. 1c.

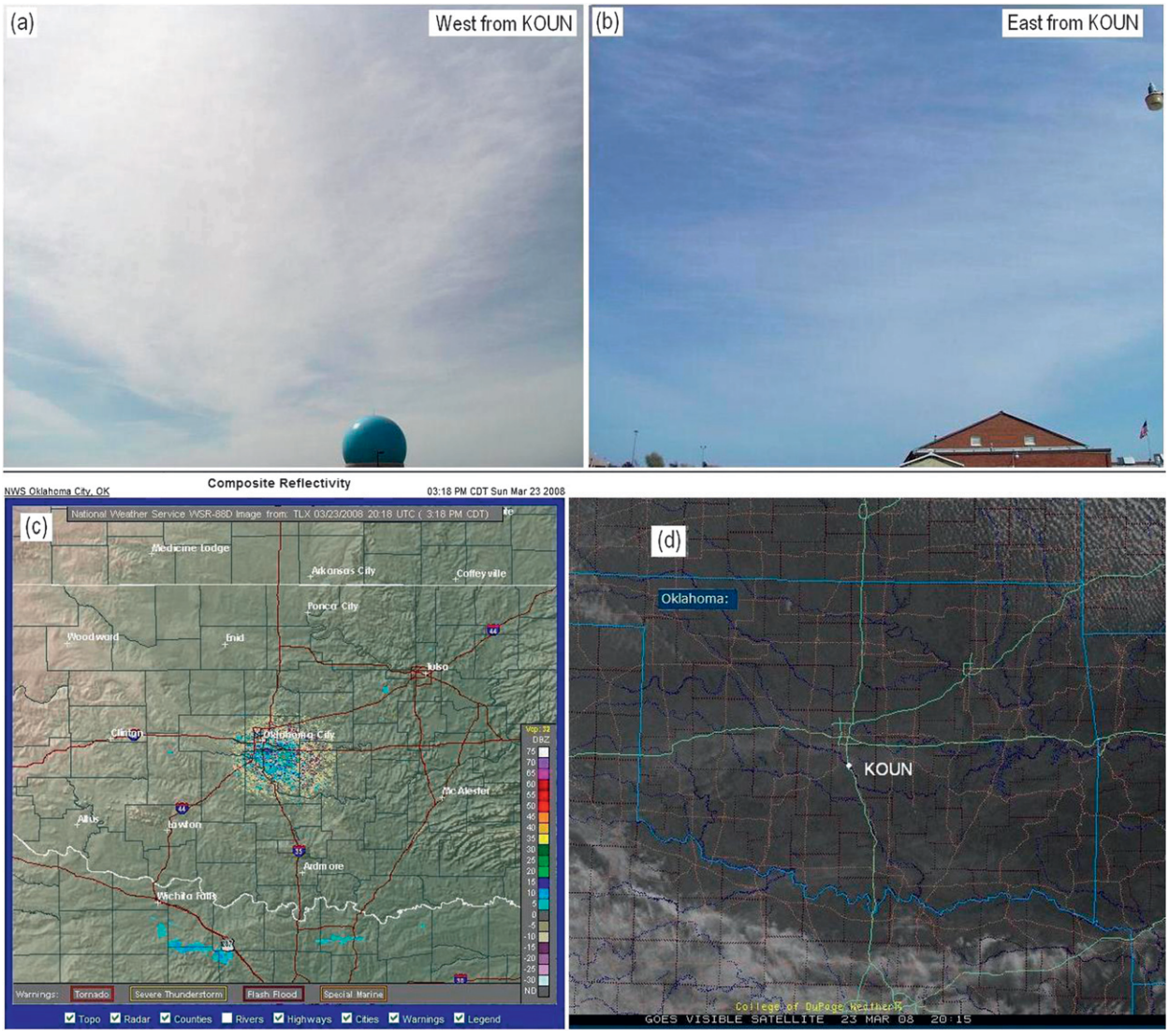

FIG. 1. The 23 Mar 2008 sky pictures from KOUN at 2021 UTC looking toward the (a) west and (b) east. (c) Composite reflectivity data from a network WSR-88D at 2018 UTC. (d) Visible satellite image of OK at 2015 UTC.

At the same time, the KOUN data from vertical cross sections at azimuth angles of 270° and 90° are presented in Figs. 2a and 2b. Cirrus clouds, at a height of about 8 km, are clearly detected to 50 km. The minimal reflectivity seen in the cirrus layer is −22.5 dBZ. Ground clutter filter residuals contaminate data to 5 km, and beyond that they are sporadic and do not pose significant problems to cloud mapping. Comparing Figs. 1c and 2, it is concluded that the signal processing and data collection procedures employed with the network WSR-88D cannot consistently show, as does the KOUN, the presence of nonprecipitating clouds.

There can be two sources of scattering of 10-cm-wavelength radiation in clouds: 1) particulate scattering and 2) Bragg scatter from turbulent fluctuations of humid air. The latter mechanism produces 0 differential reflectivity, Z_{DR}, expressed in decibels. In Fig. 2d, the field of Z_{DR} is shown. We can see that the values of Z_{DR} are positive and exceed 3 dB in the cirrus cloud bottom. High Z_{DR} values signify that at least a part of the reflected signal comes from cloud particles. Observations of positive Z_{DR} in cirrus clouds are a strong indication that ice crystals are strong sources of radar echoes at 10-cm wavelengths. In contrast to the cirrus clouds, note the convective plumes in Fig. 2b with strong reflectivities (i.e., >-5 dBZ) at their 1.5-km tops, and much weaker reflectivities in their interior regions. The plume-top differential reflectivities (Fig. 2d) are about 0 dBZ,

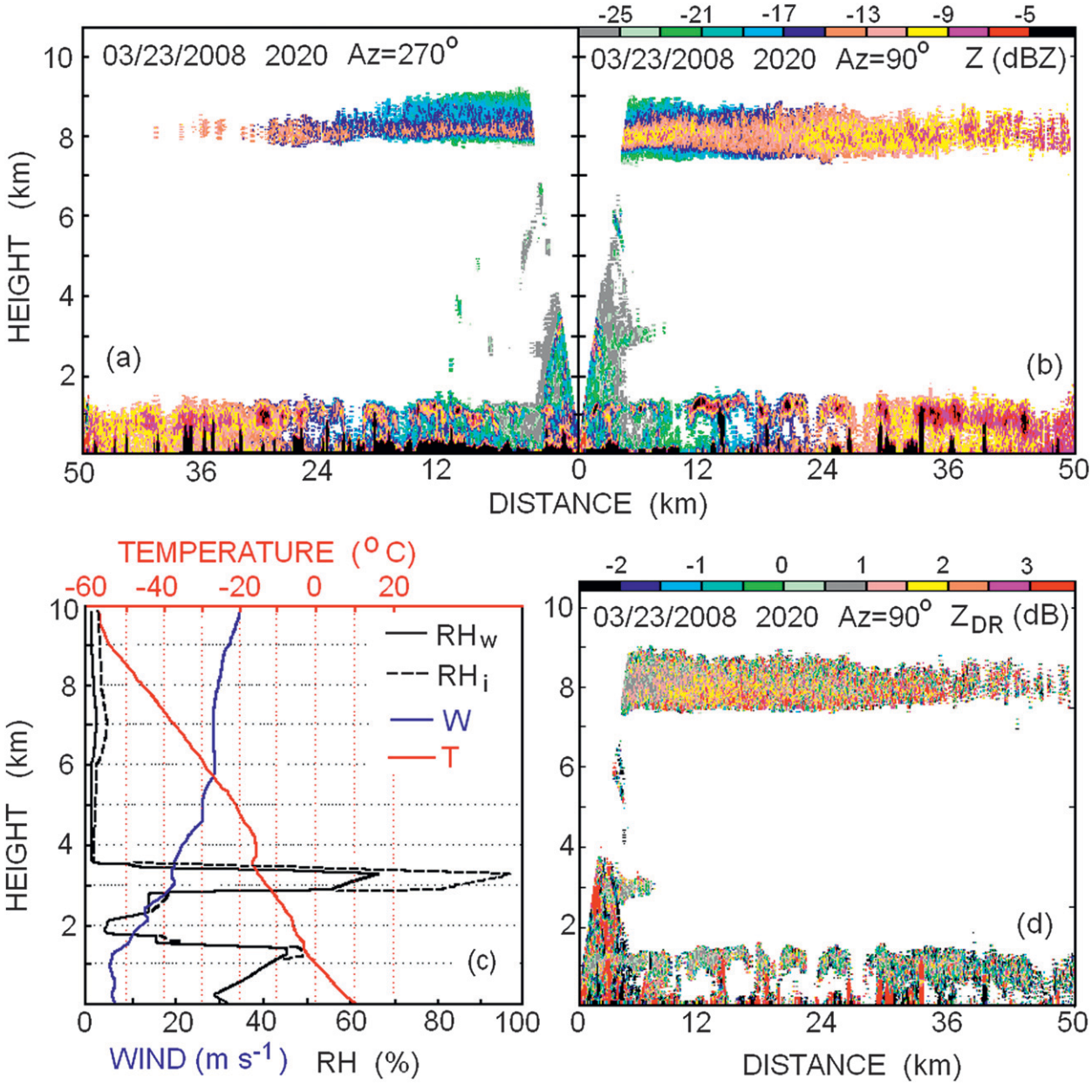

FIG. 2. Vertical cross sections of reflectivity factors observed by the KOUN radar at 2020 UTC 23 Mar 2008. SNR ≥ -7 dB for an azimuth of (a) 270° and (b) 90°. (c) Rawinsonde soundings at 0000 UTC 24 Mar 2008 of temperature (T), wind velocity (W), and relative humidity with respect to water (RH_w) and ice (RH_i) at Norman. The RH_i is shown for subfreezing temperatures. (d) Differential reflectivity field at 90° azimuth.

suggesting Bragg scatter from these regions. Detection of low-altitude clouds can be problematic in the sense of distinguishing cloud echoes from Bragg scattering in the boundary layer.

Figure 3a presents a reflectivity field with areas at the limit of KOUN's detectability. In the area shown with the arrow, at ranges of about 10 km, Z goes from -23.8 to -24.3 dBZ. Because of insertion loss from polarimetric hardware installed on research KOUN (flexible waveguides, additional length of the waveguides, insertion losses of new elements, and two rotary joints), the radar is 1.3–1.5 dB worse in terms of sensitivity when compared with the "legacy" WSR-88D. These losses will be eliminated in the dual-polarization prototype radar.

To estimate the reduction of solar radiation on the ground caused by the clouds in Figs. 1 and 2, we have

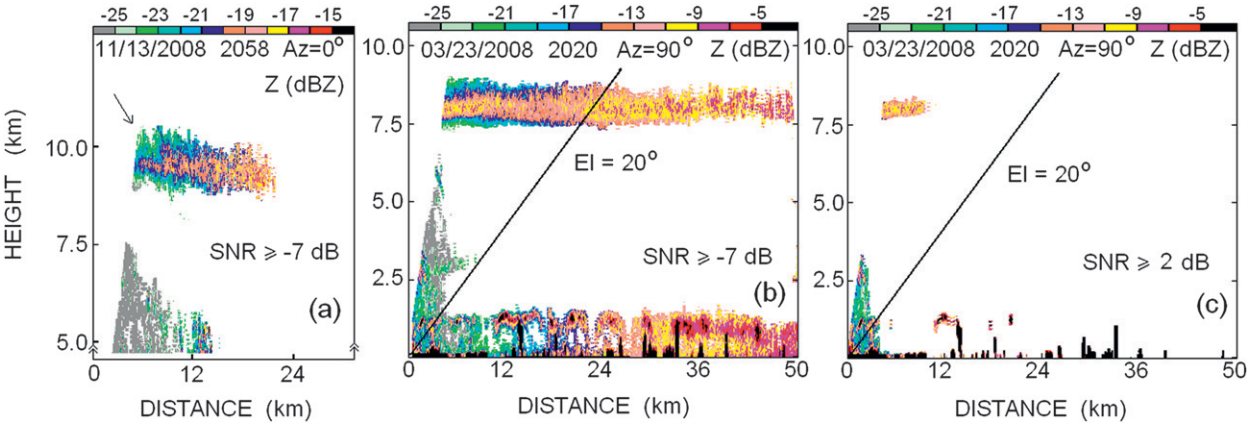

FIG. 3. (a) Vertical cross section of low reflecting clouds observed on 13 Nov 2008, and vertical cross section of reflectivity observed with the KOUN radar at 90° azimuth at 2020 UTC 23 Mar 2008 for (b) SNR ≥ -7 and (c) SNR ≥ 2 dB.

compared measured solar radiation with model results. The Bird model (Bird and Hulstrom 1981) has been used to estimate the solar flux on the ground in the absence of clouds. The Oklahoma Mesonet site in Norman measures solar radiation every 5 min. For the time represented in Fig. 2, the measured and modeled solar radiation amounts in the absence of clouds were 751 and 797 W m^{-2}, respectively. That is, the radiation deficit due to clouds was less than 6%. So we conclude that the WSR-88Ds can observe radiatively significant clouds. But to address radiation problems, it is necessary to deploy other instruments near the WSR-88D or/and satellite information should be used.

Miller et al. (1998) compared cloud detection using a WSR-88D and The Pennsylvania State University's (PSU) 3-mm-wavelength radar MMCR-3 located 18.5 km from the State College, Pennsylvania, WSR-88D (KCCX); data from the MMCR-3 were collected along a vertically directed beam to be compared with the KCCX data at various elevation angles along the same vertical. They used the WSR-88D's standard level II data collected with VCPs 11, 21, 32 (all in precipitation mode), and 31 (in clear-air mode). The level II data are an array of three meteorological variables (i.e., reflectivity factor Z; Doppler velocity v; and spectrum width σ_v) for SNR ≥ 2 dB or higher depending on the threshold settings selected by the radar operator. Miller et al. (1998), using KCCX data for SNR ≥ 6 dB, reported that the coincident detection of echoes with these radars depends on height and varies from 30% to 60%. At some times, the radars showed consistency in their detections, while at other times they did not. The discrepancies were explained by the lower sensitivity of the KCCX when this radar did not detect echoes that were recognized by PSU's MMCR-3, and by the presence of insects aloft and/or the presence of Bragg scatter to KCCX if it detected echoes that the PSU's MMCR-3 did not. On the other hand, we show that cloud observations with the WSR-88D can be carried out for SNR ≥ -7 dB, 13 dB lower than the level used in the experiments of Miller et al. (1998); so the number of cases lacking simultaneous detection could be reduced significantly.

Two RHIs shown in Figs. 3b and 3c demonstrate differences between Miller et al.'s (1998) and our experiments. Figure 3b is for the data displayed at an SNR ≥ -7 dB. Figure 3c was generated from the same data but thresholded at SNR ≥ 2 dB, the same as that for most networking WSR-88Ds, but still 4 dB lower than for the data from the experiments of Miller et al. (1998). Because of the higher SNR threshold and the use of a maximal antenna elevation of 20°, clouds would not be observed if procedures standard to the NWS operations were used. We conclude that the WSR-88D can observe many more nonprecipitating clouds than are seen routinely, but the parameters of existing VCPs are not optimal for such observations.

3. Base radar data from nonprecipitating clouds

The reflectivity factor Z, the Doppler velocity v, and the velocity spectrum width σ_v are the base radar variables measured with the WSR-88Ds. The goal of this section is to demonstrate the capability of the WSR-88D to measure and map over vast regions Z, v, and σ_v for clouds, as well as to demonstrate the need for a large unambiguous velocity for accurate measurements of v and σ_v. Often, vertical cross sections reveal important details of clouds, so herein we present vertical cross sections of the base data. Because the spectrum width cannot be accurately measured at SNR $= -7$ dB, σ_v fields are presented for an SNR ≥ -3 dB.

The detectability of clouds depends on its water–ice content and range. Often clouds are detected to ranges

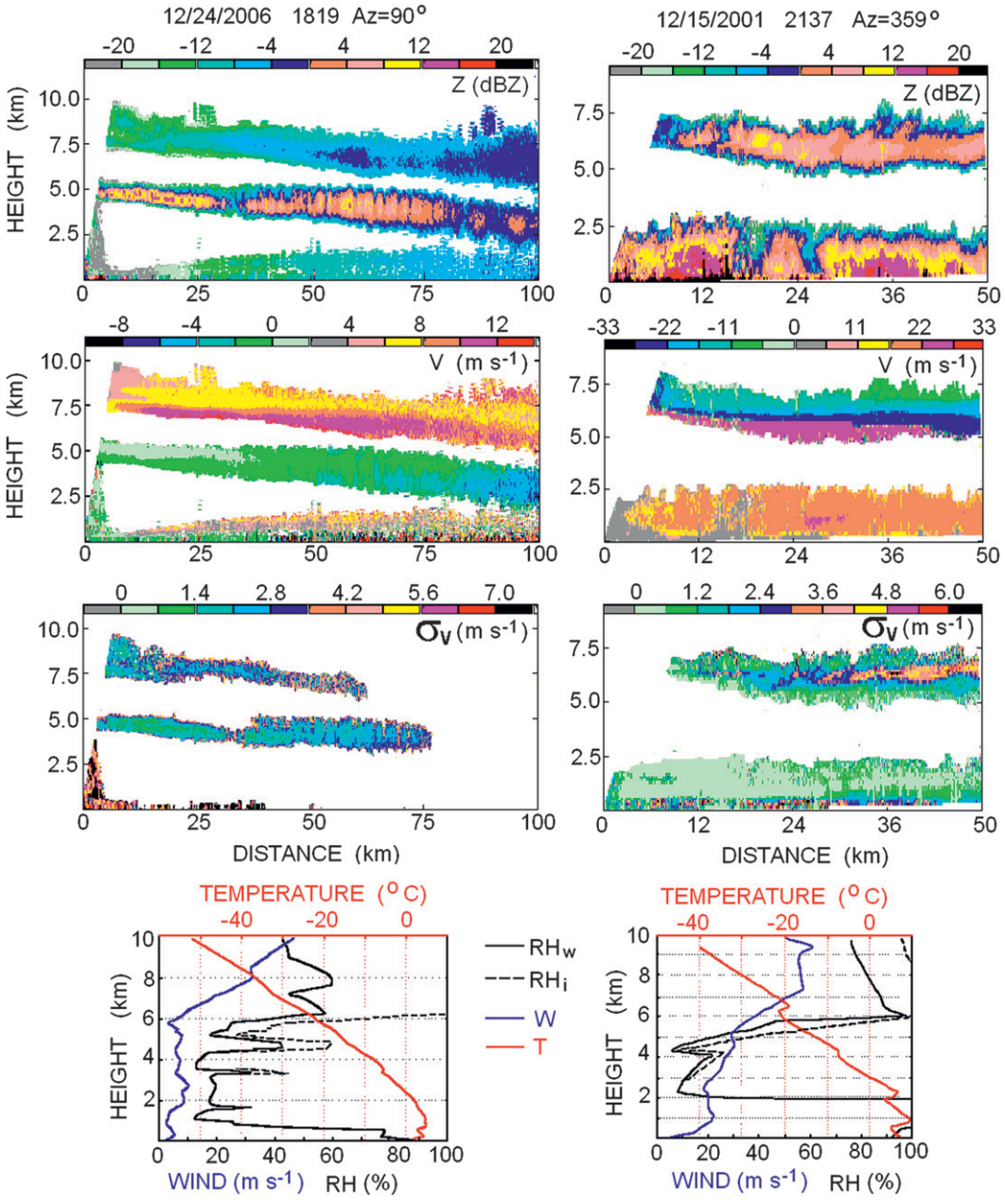

FIG. 4. Vertical cross sections of (top) reflectivity, (top middle) the Doppler velocity, and (bottom middle) spectrum width on (left) 24 Dec 2006 with two-layer nonprecipitating clouds, and (right) 15 Dec 2001 with nonprecipitating clouds above precipitation. (bottom) Temperature, wind speed, and RH profiles from rawinsondes at (left) 1200 UTC 24 Dec 2006 and (right) 0000 UTC 16 Dec 2001 at Norman.

beyond 100 km (Fig. 4, left column; Figs. 5 and 6). The two-way transversal resolution for KOUN (i.e., the square root of the second central moment of the angular weighting function) is 245 m at 50 km. Although fine features of clouds are smeared at long ranges, large-scale cloud structures are well characterized even beyond 100 km.

The left column of panels in Fig. 4 shows two layers of clouds, and the right column presents clouds above precipitation. Because 10-cm-wavelength radiation experiences negligible attenuation, the tops and bottoms of the clouds can be measured over large distances, although corrections need to be made for beam smearing at long ranges. MMCRs experience strong attenuation in dense clouds and precipitation, causing errors in defining the cloud structure. For example, in clouds with water contents of 1 g m^{-3} at 0°C, the 8- and 3-mm-wavelength

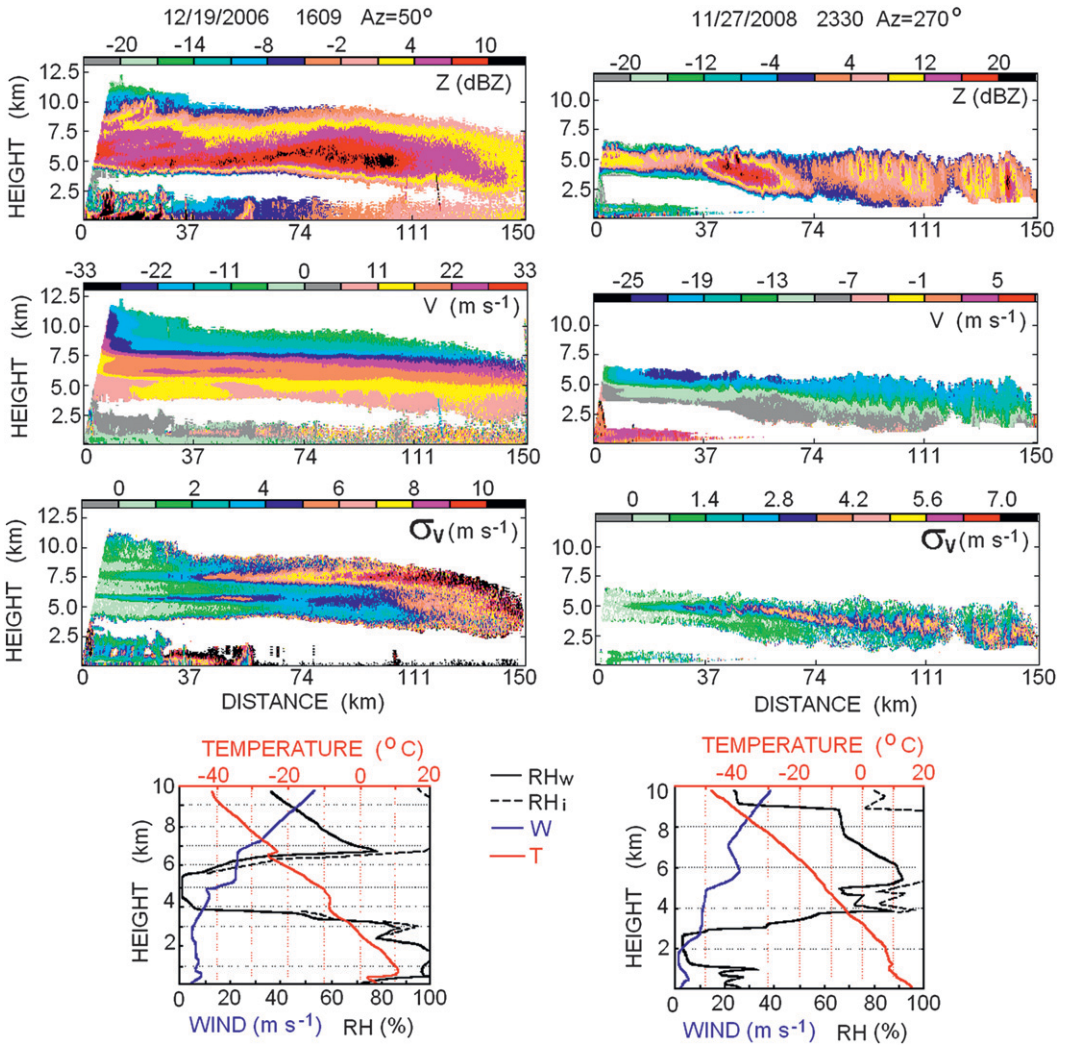

FIG. 5. As in Fig. 4, but for (left) 19 Dec 2006 and (right) 27 Nov 2008. (bottom) Data obtained at (left) 1200 UTC 19 Dec 2006 and (right) 0000 UTC 28 Nov 2008.

radiation will be attenuated by 1 and 4.8 dB km^{-1} (Meneghini and Kozu 1990, p. 152). Consider the data presented in the right column of Fig. 4 for clouds above snow falling at a rate of about 1 mm h^{-1}. Using Eq. (6.23) of Battan (1973) for 8-mm wavelength, we obtain one-way attenuation of 0.09 dB km^{-1}. At high elevation angles where the one-way path in snow is about 2 km, the total reflectivity bias of the clouds would be 0.36 dB and for a slant path of 5 km it would be 0.9 dB. But at the 3-mm wavelength, these biases would be 16 and 43 dB, considerably reducing the MMCR capability to make continuous and accurate measurements. Millimeter-wavelength radiation experiences even stronger attenuation rates in melting layers (e.g., Fig. 6h at the height of 2.7 km and Fig. 6n at 2.5 km). Thus, the WSR-88D could provide complementary information on the vertical structure of clouds and precipitation to improve the information extracted from satellite observations (e.g., Stephens and Kummerow 2007). Cloud radars are not expected to perform well in precipitation, so observations at 10-cm wavelengths are especially advantageous for studies of water accumulation in clouds and the transition to rain (e.g., thin rain shafts in Fig. 6j).

Because useful polarimetric data on cloud particles require slant soundings, and because slant soundings result in broader spectra due to the vertical shear of the horizontal wind, a large unambiguous velocity is required to accurately measure the Doppler velocity and spectrum width σ_v. One can see velocity aliasing in Fig. 4 (right, V panel) and Fig. 5 (left, V panel). At 8-mm wavelength and with a pulse repetition frequency of 3000 Hz (an unambiguous range of 50 km), the velocity would be

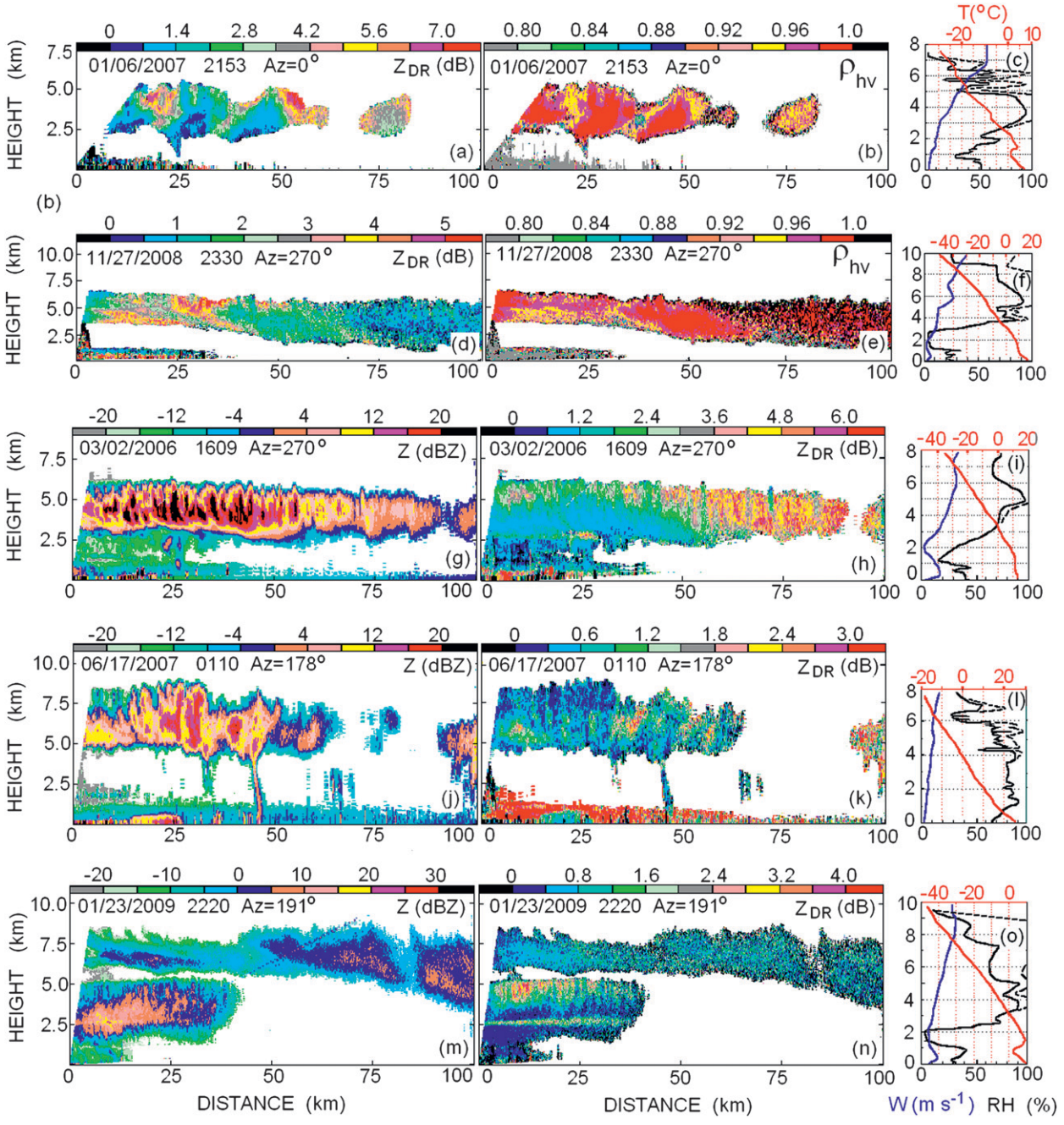

FIG. 6. Vertical cross sections of polarimetric fields. (right) Rawinsonde profiles of temperature (T), wind velocity (W), and relative humidity (RH_w and RH_i) at Norman, obtained for the closest time to radar observations: (top to bottom) 0000 UTC 7 Jan 2007, 0000 UTC 28 Nov 2008, 1200 UTC 2 Mar 2006, 0000 UTC 17 Jun 2007, and 0000 UTC 24 Jan 2009.

aliased four times, making it difficult to interpret. A higher repetition frequency would provide a larger Nyquist interval but would shorten the unambiguous range, making it even more difficult to unravel the range aliasing.

Spectrum width is related to turbulence, which is generally thought to influence the drop growth by stochastic coalescence (e.g., Jonas 1996; Shaw 2003). Waves in clouds (seen in spectrum width fields in the right σ_v panels of Figs. 4 and 5) are also significant features controlling cloud properties. To accurately measure σ_v, the unambiguous velocity must be at least 1.7 σ_v (Melnikov and Zrnić 2004). For example, the maximal measured σ_v in the cloud shown in the left σ_v panel of

Fig. 5 is 10 m s^{-1}; thus, the unambiguous velocity should be larger than 17 m s^{-1}. But wind shear, not turbulence, can be the dominant contributor to σ_v, and the narrower beams of the MMCRs can significantly reduce the shear contributions. To separate turbulence and shear contributions, a technique used by Melnikov and Doviak (2009), or that used by Hocking (2003), can be employed.

Vertical velocities in clouds are important. The WSR-88D is not capable of sounding vertically. To estimate the vertical velocities, the vertical azimuth display (VAD) technique could be used at high elevations (e.g., Doviak and Zrnić 2006, section 9.3.3). Stretching and shearing of the wind can also be obtained from the VAD data. Applications of these techniques to cloud sounding are beyond the scope of this paper. The scanning and Doppler capabilities of the WSR-88Ds allow us to determine the advection of hydrometeors, which is one of the important parameters in global cloud models. This capability could be advantageous for atmospheric radiation problems as well.

The WSR-88D network works around the clock. The mission of the network is precipitation measurements and severe weather monitoring. To not compromise that mission, cloud observations could be conducted at times without precipitation. Cloud observations can be performed with a set of vertical cross sections (i.e., RHIs). The number of RHIs that can be used to create a "cloud" VCP depends on the allowed time. In 5 min, 12 RHIs can be completed using the enhanced data acquisition and processing mode described in section 2.

4. Polarimetric radar observations of clouds

The NWS is planning to upgrade the WSR-88D network with polarimetric capabilities in the near future. The first prototype of the polarimetric WSR-88D is scheduled for deployment in 2011. The proof-of-concept WSR-88D KOUN employs a polarimetric mode with simultaneous transmission and reception of horizontally (H) and vertically (V) polarized waves (Zrnić et al. 2006). Polarimetric radar can measure more meteorological variables that can aid in retrieving cloud properties.

Simultaneously with the base radar variables, KOUN routinely measures the following polarimetric variables: 1) differential reflectivity Z_{DR}, 2) total differential phase ϕ_{DP}, and 3) the copolar correlation coefficient ρ_{hv} (e.g., Doviak and Zrnić 2006, section 6.8). KOUN also has the capability of switching from transmitting H only to also measuring the cross-polar coefficients. Signals from clouds are often weak, and thus the influence of noise on polarimetric variables can be strong. To mitigate the noise impacts at low SNR, the covariance estimators of polarimetric variables are used in the KOUN (Melnikov and Zrnić 2007). The polarimetric radar variables are measured during the same dwell time as that for the base radar variables.

Observations of nonprecipitating clouds with KOUN show a tremendous amount of information in the fields of polarimetric variables. In this paper, we do not analyze the polarimetric fields in detail but rather show their main features to suggest the wealth of information that could be derived from these variables. There is no correlation between reflectivity and differential reflectivity in clouds (see, e.g., Figs. 6g and 6h, 6j and 6k, and 6m and 6n) in contrast to rain wherein Z and Z_{DR} are positively correlated (e.g., Doviak and Zrnić 2006, section 8.5.3). The correlation for rain occurs because more intense rain typically has larger drops that are oblate and thus correspondingly larger Z_{DR}. Figure 7a presents a scatterplot of Z and Z_{DR} in clouds shown in Figs. 6g and 6h wherein the lack of correlation between the variables for clouds is apparent. In Fig. 7b, a scatterplot of Z_{DR} and ρ_{hv} also shows weak negative correlation, and ρ_{hv} as low as 0.9, which is again in contrast to rain wherein ρ_{hv} is typically larger than 0.98. The lack of correlation between Z, Z_{DR}, and ρ_{hv} in clouds is due to the presence of ice particles, which can have random orientation. Furthermore, Z_{DR} could decrease with increasing Z due to the aggregation of ice particles; that is, the aggregates are more spherical (i.e., have lower Z_{DR} but larger Z) than the particles they consist of.

In some clouds, fields of differential reflectivity are uniform with values lower than 1 dB; the Z_{DR} field in Fig. 2d is nearly uniform but has values substantially exceeding 1 dB, which suggests scatter from ice particles. Often, Z_{DR} exhibits a wide range of values (i.e., 0–8 dB; e.g., the maximal Z_{DR} in Fig. 6a is 8.3 dB), and exhibits patterns with "pockets" of high and low Z_{DR}, as in Figs. 6a, 6d, 6h, and 6k), suggesting differing processes of formation and evolution of hydrometeors. The observed positive Z_{DR} in clouds also indicates that particles make a strong contribution to echoes although a contribution from Bragg scatter could exist.

Observations from KOUN show high temporal variability of the polarimetric fields. Rapid changes in the polarimetric variables could be linked to crucial microphysical processes. Thus, having a rapid-scan polarimetric Doppler radar could prove valuable for microphysical analyses. Polarimetric radar at 10-cm wavelengths can be a powerful tool to complement MMCR radar studies of clouds with mixed phases, which are challenges for remote sensors (e.g., Shupe et al. 2008).

Polarimetric information is successfully used in classifying various types of scatterers in the atmosphere. For example, the polarimetric variables Z_{DR} and ρ_{hv} can be

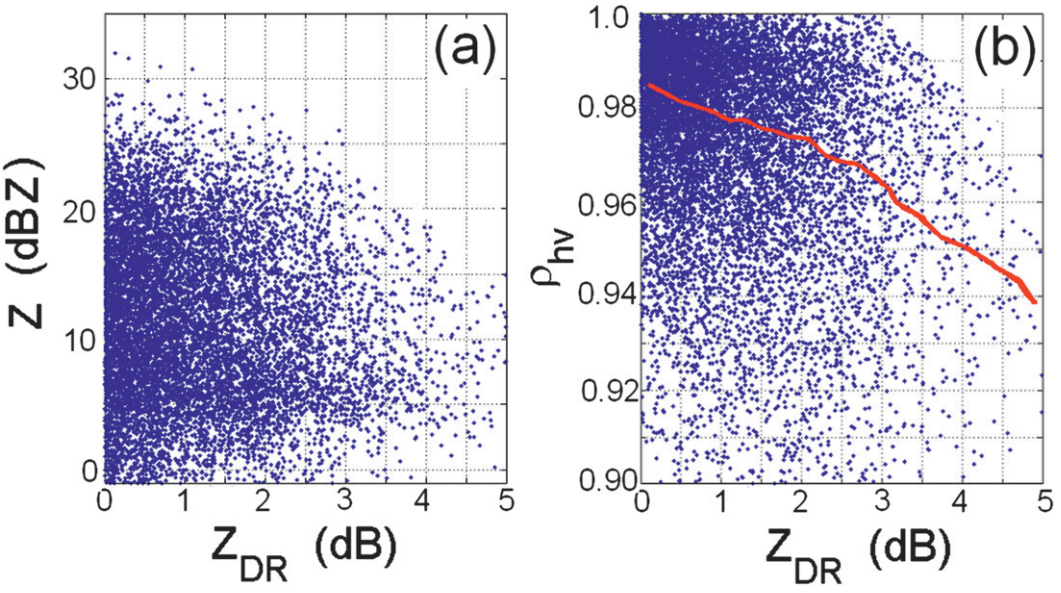

FIG. 7. Scatterplots of measured Z, Z_{DR}, and ρ_{hv} for clouds shown in Figs. 6g and 6h. The red line in (b) is the median obtained from the radar data.

used to distinguish hydrometeor and biological scatterers (e.g., insects and birds; Zrnić and Ryzhkov 1999). Measurement of Z_{DR} and ρ_{hv} is most suitable for slant soundings of the atmosphere because polarimetric measurements lose much of their value for vertical soundings. Furthermore, it is important to have low attenuation of radiation, as it is for 10-cm wavelengths, to be sure that differential attenuation does not modify Z_{DR}. Thus, the WSR-88D is well suited for polarimetric observations in clouds and should complement measurements with MMCRs.

5. Resolving scatter mechanisms in clouds

Many visual cloud images from the ground and satellites exhibit good correspondence with radar-derived images. But these observations do not prove that echoes come exclusively from cloud particles. Knight and Miller (1993, 1998) studied dual-wavelength (i.e., 10 and 3 cm) reflectivity data from the early stages of convective clouds, and deduced that there are at least two sources of backscatter signals: Rayleigh scatter from cloud droplets and coherent or Bragg scatter from refractive index variations (see also Gossard 1979). They found that Bragg scatter from developing cumulus clouds can dominate Rayleigh scatter at 10-cm wavelengths. Resolving Bragg and particulate scatter in precipitation was considered by Gage et al. (1999). The purpose of this section is to show how polarimetric radar can be helpful in resolving these two types of scattering mechanisms.

To differentiate classical Bragg scatter associated with a fixed arrangement of scatters from the Bragg scatter associated with random changes in density perturbations, Bragg scatter from refractive index perturbations has been defined as stochastic Bragg scatter (Doviak 1999) or as stochastically coherent scatter (Zhang et al. 1990; Erkelens et al. 2001). Comparing radar returns at 10- and 0.9-cm wavelengths, Kropfli and Kelly (1996) also suggested that fluctuations of refractivity caused by developing cumulus clouds can contribute significantly to backscatter at 10-cm wavelengths. Whereas these studies showed significant Bragg scatter from cumulus clouds at 10-cm wavelength, Gossard and Strauch (1981), using 3-cm-wavelength radar, found no evidence of Bragg scatter from stratiform clouds.

The Bragg scatter from air and its corresponding reflectivity η_a is (e.g., Ottersten 1969; Doviak and Zrnić 2006, section 11.4.3.1)

$$\eta_a = \frac{0.38C_n^2}{\lambda^{1/3}}, \tag{1}$$

where λ is the radar's wavelength and C_n^2 is the atmosphere's refractive index structure parameter. The received voltage V associated with backscatter from cloud particles is proportional to $V = \sum_n a_n \exp(2jkr_n)$, where $k = 2\pi/\lambda$ is the propagation wavenumber; a_n is the contribution from, and r_n the range to, the nth particle; and the summation includes all particles having significant return. The ensemble average power is [Doviak and Zrnić 2006, Eq. (4.2); Siegert and Goldstein 1951]

$$P = E[|V|^2]$$
$$= E\left[\sum_n |a_n|^2\right] + E\left[\sum_{n\neq m} a_n a_m^* \exp[2jk(r_n - r_m)]\right]$$
$$= \frac{A}{r^2}(\eta_{pi} + \eta_{pc}), \quad (2)$$

where $E[x]$ represents an ensemble or time average, A is a radar constant, the asterisk denotes a complex conjugate, r is the range to the scattering volume, and the total reflectivity (i.e., the scatter cross section per unit volume), $\eta_p \equiv \eta_{pi} + \eta_{pc}$, is composed of reflectivities η_{pi} and η_{pc} due to incoherent and coherent scatter from particles (i.e., hydrometeors). If the scatterer's locations are uncorrelated, the ensemble average of the second summation is zero (i.e., $\eta_{pc} = 0$), and there remains only the commonly observed incoherent hydrometeor backscatter.

But if there is spatial correlation of scatterer locations (i.e., random density perturbations at two locations are correlated), then the ensemble average of the second term is not 0. If the density perturbations have strong spatial variations at $\lambda/2$ scales, there will be correspondingly strong coherent scatter from the hydrometeor's density fluctuations; note in (2) that there are N^2 terms contributing to the coherent term compared to N terms for incoherent scatter. Although reflectivity associated with stochastic Bragg scatter can be large compared to that associated with incoherent scatter, the evidence for strong Bragg scatter from perturbations in hydrometeor number density is spotty (e.g., Erkelens et al. 2001).

The incoherent component of reflectivity $\eta_{pi}^{h,v}$ for horizontally or vertically polarized waves is (Doviak and Zrnić 2006, section 8.5.3.1)

$$\eta_{pi}^{h,v} = \frac{\pi^5 |K|^2}{\lambda^4} Z_{h,v}, \quad (3)$$

where K is the dielectric factor of the hydrometeor and $Z_{h,v}$ are the reflectivity factors of the hydrometeors for horizontal or vertical polarization. Erkelens et al. (2001) and Gossard and Strauch (1983, section 2.5) hypothesized that turbulence, mixing mean gradients of particulate density N_p, creates stochastic Bragg scatter reflectivity expressed as

$$\eta_{pc} = \frac{0.38 C_p^2}{\lambda^{1/3}}, \quad (4)$$

where C_p^2 is the structure parameter of the hydrometeor density perturbations. Using simplifying assumptions (i.e., all particles are spherical and have the same diameter, the inertial subrange of turbulence extends to scales at least as small as $\lambda/2$, and ignoring evaporation and condensation), Erkelens et al. (2001) show that $C_p^2 = 3.39|K|^2 L_0^{-2/3} \beta^2 E[N_p^2] D^6$, where L_0 is the outer scale of turbulence, D is the particles' diameter, and β^2 is a proportionality parameter relating the variance of η_p to $E[N_p^2]$. Parameter C_p^2 can be expressed in terms of Z by noting that $Z = E[N_p] D^6$. Therefore, $C_p^2 = 3.39|K|^2 qZ$, where $q = L_0^{-2/3} \beta^2 E[N_p^2]/E[N_p]$ is a combined unknown.

The total reflectivity η is simply the sum of the reflectivities (i.e., $\eta_{pi} + \eta_a + \eta_{pc}$) for each of the three scattering mechanisms. That is,

$$\eta = \frac{\pi^5 |K|^2 Z}{\lambda^4} + \frac{0.38 C_n^2}{\lambda^{1/3}} + \frac{3.39|K|^2 qZ}{\lambda^{1/3}}. \quad (5)$$

Because Bragg scatter from hydrometeors has the same wavelength dependence as that from the refractive index, we can use data from radars operating at different wavelengths (e.g., 3 and 10 cm) to calculate Z, the reflectivity factor associated with the hydrometeors.

Equation (5) also applies to nonspherical particles such as ice crystals for which $Z_h \neq Z_v$. In this case there are four unknowns: Z_h, Z_v, C_n^2, and q. To solve for them, we can apply polarimetric measurements at two wavelengths. Because Bragg scatter from refractive index perturbations has no differential reflectivity, we deduce

$$\eta_h = \frac{\pi^5 |K|^2 Z_h}{\lambda^4} + \frac{0.38 C_n^2}{\lambda^{1/3}} + \frac{3.39|K|^2 qZ_h}{\lambda^{1/3}} \quad \text{and} \quad (6a)$$

$$\eta_v = \frac{\pi^5 |K|^2 Z_v}{\lambda^4} + \frac{0.38 C_n^2}{\lambda^{1/3}} + \frac{3.39|K|^2 qZ_v}{\lambda^{1/3}}. \quad (6b)$$

At centimeter wavelengths, cloud particles can be considered to be Rayleigh scatterers. Therefore, the measured reflectivity factors Z_h and Z_v are equal at different wavelengths, λ_1 and λ_2 [e.g., $Z_h(\lambda_1) = Z_h(\lambda_2)$]. Measurements at two wavelengths and two polarizations are sufficient to calculate all four unknowns. But (6) assumes that inertial subrange turbulence, responsible for Bragg scatter, is present at both wavelengths.

The purpose of suggesting a dual-wavelength, dual-polarization experiment is to establish whether Bragg scatter from stratiform clouds is significant. Gossard and Strauch (1981) found no evidence of Bragg scatter from stratiform clouds at 3-cm wavelengths, but this has not been established for 10-cm wavelengths. If Bragg scatter from stratiform clouds is insignificant, then the dual-polarization WSR-88D can provide reliable and accurate data on cloud particles.

Polarimetric radar observations with KOUN show that at the same height in a cloud, differential reflectivity can vary by few decibels (Fig. 6). Hydrometeor scatter must dominate in regions with high Z_{DR} because scatter

from refractive index perturbations has $Z_{DR} = 0$ dB. The observed positive Z_{DR} in stratiform clouds strongly suggests particles are one of the main sources of radar echoes from such clouds.

6. Conclusions

Our observations with the KOUN WSR-88D using enhanced signal processing show sufficient sensitivity of the radar for measurements of various cloud parameters. We have observed, in a dual-polarization mode, reflectivities as low as −23 dBZ at 10-km ranges; the total reflectivity span is about 58 dB in nonprecipitating clouds. The ground-based cloud radars have 3–5 times superior spatial resolution. Our cloud observations with the KOUN radar show that within 50 km the spatial resolution of KOUN is satisfactory to measure the spatial structure of most clouds. Smearing of radar fields is seen at longer ranges but the main features of radar fields are still preserved. Observations with the KOUN radar showed the great advantages of scanning radars—''instant'' fields of cloud properties are obtained and patterns of the time evolution of the fields are observed.

Wind and turbulence strongly affect microphysical processes in clouds, so Doppler measurements are important. To measure wind shears and turbulence with scanning radars (i.e., beams not vertically directed), a wide unambiguous Doppler velocity interval is required. The WSR-88D is well suited for Doppler measurements and could supplement data collected with MMCRs.

Additional information on the microphysics of cloud particles can be obtained with radar polarimetry, especially at elevation angles far from zenith. The planned polarimetric upgrades to the WSR-88D will provide the capability to measure reflectivity factors as low as −25.5 dBZ. Thus, the WSR-88D could be a valuable supplement to cloud measurements with MMCRs. The WSR-88D is well suited for polarimetric observations: 10-cm-wavelength radiation does not experience attenuation in clouds and light precipitation, so measured parameters are not biased by attenuation. At millimeter wavelengths, attenuation is an issue.

Polarimetric observations of nonprecipitating clouds conducted with the KOUN WSR-88D show a tremendous amount of information on polarimetric variables. In clouds, the differential reflectivity Z_{DR} spreads over a wide interval from 0 to over 8 dB, which is much wider than in rain. Because of the ice phase, there is no clear Z–Z_{DR} relation as there is for rain. In some clouds, Z_{DR} fields are uniform but more frequently they exhibit patterns with ''pockets'' of high and low Z_{DR}; this likely points to intense processes of transformation of hydrometeors.

Our observations of positive Z_{DR} in stratiform clouds suggest that particles are one of the main sources of radar echoes at 10-cm wavelengths. It is suggested that simultaneous observations with 3- and 10-cm polarimetric radars would be capable of relating the measured power to the reflectivity factor Z of cloud particles. Furthermore, the addition of dual-wavelength observations could quantify the relative importance of Bragg scatter from the fluctuations in hydrometeor density and the fluctuations in air density (i.e., in refractive index). Bragg scatter from air could bias Z_{DR} toward 0 dB. Thus, the presence of cloud areas with large positive Z_{DR} in clouds points to the absence of significant Bragg scatter at least in those areas.

Cloud data from WSR-88Ds can be used in studies of the development and evolution of clouds and precipitation, cloud model parameterization, radiation transfer in cloudy atmospheres, and as an instrument in climatic cloud studies. The radar is not capable of sampling all of the radar-radiatively significant clouds but it is possible to collect radar data from cirrus clouds that reduce the solar flux reduction on the ground by up to 6%. The radar is also capable of estimating the advection of hydrometeors, which is an important parameter in radiation transfer problems.

The NWS WSR-88Ds work around the clock. Because many days in a year are cloudy without precipitation, these WSR-88Ds can be used for cloud observations without compromising their primary mission. Cloud observations with the WSR-88Ds can be implemented into the existing radar network and could make the network an instrument for climate studies.

Acknowledgments. Mr. M. Schmidt and Mr. R. Wahkinney maintained the WSR-88D KOUN in impeccable condition. We thank Dr. G. Zhang and our anonymous reviewers for their critical review and suggestions that helped us to improve the manuscript. We also thank Dr. C. A. Fiebrich and Ms. A. G. McCombs for their assistance with data from the Oklahoma Mesonet. Funding for this study was provided by the NOAA/Office of Oceanic and Atmospheric Research under NOAA–University of Oklahoma Cooperative Agreement NA17RJ1227 (U.S. Department of Commerce).

REFERENCES

Battan, L. J., 1973: *Radar Observation of the Atmosphere*. University of Chicago, 324 pp.

Bird, R. E., and R. L. Hulstrom, 1981: A simplified clear sky model for direct and diffuse insolation on horizontal surfaces. Solar Energy Research Institute Tech Rep. SERI/TR-642-761, 39 pp.

Clothiaux, E. E., M. A. Miller, B. A. Albrecht, T. P. Ackerman, J. Verlinde, D. M. Babb, R. M. Peters, and W. J. Syrett, 1995:

An evaluation of a 94-GHz radar for remote sensing of cloud properties. *J. Atmos. Oceanic Technol.,* **12,** 201–229.

Doviak, R. J., 1999: Scattering from refractive index perturbations in turbulent flow. [Published lecture available from the National MST Radar Facility, Gandanki-517 122, Tirupati, India.]

——, and D. S. Zrnić, 2006: *Doppler Radar and Weather Observations*. 2nd ed. Dover, 562 pp.

Erkelens, J. S., V. K. C. Venema, H. W. J. Russchenberg, and L. P. Ligthart, 2001: Coherent scattering of microwaves by particles: Evidence from clouds and smoke. *J. Atmos. Sci.,* **58,** 1091–1102.

Gage, K. S., C. R. Williams, W. L. Ecklund, and P. E. Johnston, 1999: Use of two profilers during MCTEX for unambiguous identification of Bragg scattering and Rayleigh scattering. *J. Atmos. Sci.,* **56,** 3679–3691.

Gossard, E. E., 1979: A fresh look at the radar reflectivity of clouds. *Radio Sci.,* **14,** 1089–1097.

——, and R. G. Strauch, 1981: The refractive index spectra within clouds from forward-scatter radar observations. *J. Appl. Meteor.,* **20,** 170–183.

——, and ——, 1983: *Radar Observations of Clear Air and Clouds*. Elsevier, 280 pp.

Hamazu, K., H. Hashiguchi, T. Wakayama, T. Matsuda, R. J. Doviak, and S. Fukao, 2003: A 35-GHz scanning Doppler radar for fog observations. *J. Atmos. Oceanic Technol.,* **20,** 972–986.

Hocking, W. K., 2003: Fast and accurate calculation of spectral beam-broadening for turbulence studies. *Proc. 10th Int. Workshop on Technical and Scientific Aspects of MST Radar,* Piura, Peru, International Union of Radio Science, 214–217.

Jonas, P. R., 1996: Turbulence and cloud microphysics. *Atmos. Res.,* **40,** 283–306.

Knight, C. A., and L. J. Miller, 1993: First radar echoes from cumulus clouds. *Bull. Amer. Meteor. Soc.,* **74,** 179–188.

——, and ——, 1998: Early radar echoes from small, warm cumulus: Bragg and hydrometeor scattering. *J. Atmos. Sci.,* **55,** 2974–2992.

Kollias, P., B. A. Albrecht, R. Lhermitte, and A. Savtchenko, 2001: Radar observations of updrafts, downdrafts, and turbulence in fair-weather cumuli. *J. Atmos. Sci.,* **58,** 1750–1766.

——, E. E. Clothiaux, M. A. Miller, B. A. Albrecht, G. L. Stephens, and T. P. Ackerman, 2007: Millimeter-wavelength radars: New frontier in atmospheric cloud and precipitation research. *Bull. Amer. Meteor. Soc.,* **88,** 1608–1624.

Kropfli, R. A., and R. D. Kelly, 1996: Meteorological research applications of mm-wave radar. *Meteor. Atmos. Phys.,* **59,** 105–121.

Manheimer, W. M., and Coauthors, 2003: Initial cloud images with the NRL high power 94 GHz WARLOC radar. *Geophys. Res. Lett.,* **30,** 1103, doi:10.1029/2002GL016507.

Matrosov, S. Y., T. Uttal, J. B. Snider, and R. A. Kropfli, 1992: Estimates of ice cloud parameters from ground-based infrared radiometer and radar measurements. *J. Geophys. Res.,* **97,** 11 567–11 574.

——, A. Korolev, and A. J. Heymsfield, 2002: Profiling ice mass and characteristic particle size from Doppler radar measurements. *J. Atmos. Oceanic Technol.,* **19,** 1003–1018.

Melnikov, V., and D. S. Zrnić, 2004: Estimates of large spectrum widths from autocovariances. *J. Atmos. Oceanic Technol.,* **21,** 969–974.

——, and ——, 2007: Autocorrelation and cross-correlation estimators of polarimetric variables. *J. Atmos. Oceanic Technol.,* **24,** 1337–1350.

——, and R. J. Doviak, 2009: Turbulence and wind shear in layers of large Doppler spectrum width in stratiform precipitation. *J. Atmos. Oceanic Technol.,* **26,** 430–443.

Meneghini, R., and T. Kozu, 1990: *Spaceborne Weather Radar*. Artech House, 199 pp.

Miller, M. A., J. Verlinde, G. V. Gilbert, G. J. Lehenbauer, J. S. Tongue, and E. E. Clothiaux, 1998: Detection of nonprecipitating clouds with the WSR-88D: A theoretical and experimental survey of capabilities and limitations. *Wea. Forecasting,* **13,** 1046–1062.

Moran, K. P., B. E. Martner, M. J. Post, R. A. Kropfli, D. C. Welsh, and K. B. Widener, 1998: An unattended cloud profiling radar for use in climate research. *Bull. Amer. Meteor. Soc.,* **79,** 443–455.

Ottersten, H., 1969: Atmospheric structure and radar backscattering in clear air. *Radio Sci.,* **4,** 1179–1193.

Reinking, R. F., S. Y. Matrosov, R. A. Kropfli, and B. W. Bartram, 2002: Evaluation of a 45° slant quasi-linear radar polarization state for distinguishing drizzle droplets, pristine ice crystals, and less regular ice particles. *J. Atmos. Oceanic Technol.,* **19,** 296–321.

Shaw, R. A., 2003: Particle–turbulence interactions in atmospheric clouds. *Annu. Rev. Fluid Mech.,* **35,** 183–227.

Shupe, M. D., and Coauthors, 2008: A focus on mixed-phase clouds. *Bull. Amer. Meteor. Soc.,* **89,** 1549–1562.

Siegert, A. F. G., and H. Goldstein, 1951: Coherent and incoherent scattering from assemblies of scatterers. *Propagation of Short Radio Waves,* D. E. Kerr, Ed., McGraw-Hill, 699–706.

Stephens, G. L., and C. D. Kummerow, 2007: The remote sensing of clouds and precipitation from space: A review. *J. Atmos. Sci.,* **64,** 3742–3765.

——, and Coauthors, 2002: The *CloudSat* mission and the A-Train. *Bull. Amer. Meteor. Soc.,* **83,** 1771–1790.

Widener, K. B., and J. B. Mead, 2004: W-band ARM cloud radar—Specifications and design. *Proc. 14th ARM Science Team Meeting,* Albuquerque, NM, Department of Energy/Office of Science. [Available online at http://www.arm.gov/publications/proceedings/conf14/.]

Zhang, G., J. Hou, S. Ito, and T. Oguchi, 1990: Optical wave propagation in random medium composed of both turbulence and particles. *J. Commun. Res. Lab.,* **37** (151/152), 43–62.

Zrnić, D. S., and A. V. Ryzhkov, 1999: Polarimetry for weather surveillance radars. *Bull. Amer. Meteor. Soc.,* **80,** 389–406.

——, V. M. Melnikov, and J. K. Carter, 2006: Calibrating differential reflectivity on the WSR-88D. *J. Atmos. Oceanic Technol.,* **23,** 944–951.